LPC CAEN

Directed collective flow and azimuthal distributions in ^{36}Ar + ^{27}Al collisions from 55 to 95 MeV/u

J.C. Angélique, A. Buta, G. Bizard, D. Cussol, A. Péghaire, J. Péter, R. Popescu,

G. Auger, R. Brou, C. Cabot, E. Crema, Y. El Masri, P. Eudes, Z.Y. He,

A. Kerambrun, C. Lebrun, R. Regimbart, E. Rosato, F. Saint-Laurent,
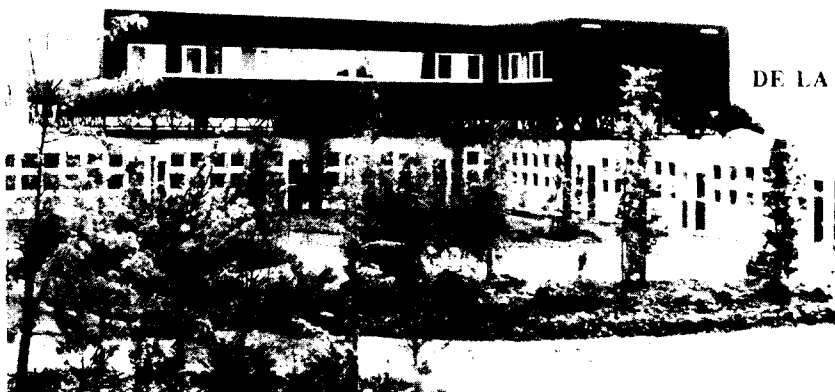
J.C. Steckmeyer, B. Tamain, E. Vient

DIRECTED COLLECTIVE FLOW AND AZIMUTHAL DISTRIBUTIONS IN ^{36}Ar + ^{27}Al COLLISIONS FROM 55 TO 95 MeV/U * .

J.C. Angélique[1], A. Buta[1-a], G. Bizard[1], D. Cussol[1],
A. Péghaire[2], J. Péter[1], R. Popescu[1-a],
G. Auger[2], R. Brou[1], C. Cabot[2-c], E. Crema[2-b], Y. El Masri[3], P. Eudes[4], Z.Y. He[6],
A. Kerambrun[1], C. Lebrun[4], R. Regimbart[1], E. Rosato[5], F. Saint-Laurent[2],
J.C. Steckmeyer[1], B. Tamain[1], E. Vient[1]

1) LPC Caen, ISMRA, IN2P3-CNRS, Bd Maréchal Juin, 14050 CAEN CEDEX, FRANCE
2) GANIL, BP 5027, 14021 CAEN CEDEX, FRANCE
3) Institut de Physique Nucléaire, UCL, 1348 LOUVAIN-LA-NEUVE, BELGIUM
4) Laboratoire de Physique Nucléaire, 44072 NANTES CEDEX 03, FRANCE
5) Dipartimento di Scienze Fisiche and INFN, Univ. di Napoli, 80125 NAPOLI, ITALY
6) Institute of Modern Physics, LANZHOU 730000, CHINA

a) Permanent address : I.F.A., Heavy Ion Department, BUCHAREST, ROMANIA
b) Permanent address : Inst. di Fisica, Univ. de SAO PAULO, BRAZIL
c) On leave of absence from IPN ORSAY, France

Abstract

A 4π charged particle detector array with a low velocity threshold has been used to detect the products from reactions induced by ^{36}Ar on ^{27}Al at energies ranging from 55 to 95 MeV/u. Well characterized events were selected and sorted as a function of the impact parameter. Two methods were used for sorting these events with respect to their impact parameters and three methods were compared to determine the reaction plane. The transverse momentum analysis has been found to be the best method to extract the direction of the reaction plane for this system and for the experimental set-up used here. The energy of vanishing flow for central collisions has been found to be around 90-95 MeV/u. The azimuthal distributions of mid-rapidity particles exhibit a preferential in-plane emission and no squeeze-out effect.

1 Motivations

The collective motion of particles emitted in the first steps of nucleus-nucleus collisions (pre-equilibrium particles) provides information on the nuclear equation of state (incompressibility modulus K) and on the nucleon-nucleon cross section in matter [1, 2]. The momentum distribution of the emitted nucleons may be approximated as a spheroidal shape. This shape has been fully studied in a few cases [3], but its main features can be expressed via two quantities : the flow angle, which characterizes the average deflection of the pre-equilibrium nucleons, and the shape of their azimuthal distribution.

---

* Experiment performed at the GANIL accelerator

1

The shape of the spheroid is obtained via momentum tensor analysis. The main axis is, for symmetry reasons, located in the reaction plane and its angle with the beam direction is the flow angle. However, the construction of the spheroid for each event is difficult for several reasons : i) at large and low rapidities, pre-equilibrium particles are not separated from particles emitted at later stages; ii) detection thresholds cut a part of the low rapidity particles; iii) for light systems and/or low energies , the number of pre-equilibrium nucleons is small. Therefore, it is generally easier and more accurate to determine the value of the flow parameter which is obtained via transverse momentum analysis [4].

The collective flow studied here is the directed in-plane (or sidewards) flow, not to be confused with the expansion flow [5]. At large incident energies, the flow is positive, i.e. the particles emitted at forward angles are on the average deflected to the same side as the projectile, due to the dominance of repulsive nucleon-nucleon interactions. Conversely, at low energy mean field attraction gives birth to negative flow. The energy of vanishing flow [6], also called balance energy [7] varies from 30 MeV/u for very heavy systems, up to 120 MeV/u for the $^{12}C+^{12}C$ system [6, 7] .

The azimuthal distribution of particles at the center-of-mass rapidity has been found to be characterized by an enhancement in the direction perpendicular to the reaction plane, the so-called squeeze-out effect, at high energies [8]. At low energies, an in-plane enhancement was attributed to rotational-like behaviour [9, 10]. The transition from in-plane to out-of-plane enhancement has been studied as a function of incident energy, impact parameter and charge of the product [11].

For these studies the reaction plane direction is needed. Its determination is always subject to some error, even with a perfect detector, due to the finite number of nucleons. Since the flow helps to determine the reaction plane, the error is larger when the flow parameter has a small value [12].

Recently azimuthal correlations, which do not require the knowledge of the reaction plane, have been shown to provide useful information on the characteristics of flow [13, 14]. Specifically, the energy of vanishing flow and the energy of uniform azimuthal distribution can be determined by studying these correlations as a function of incident energy [15].

In this paper we report on an experimental study conducted with the 4π array MUR + TONNEAU in the reaction chamber NAUTILUS on the system $^{36}Ar+^{27}Al$ from 55 to 95 MeV/u (maximum energy available at GANIL). Partial results on the close system $^{40}Ar+$ ^{27}Al from 35 to 85 MeV/u were published already [10, 16]. Theoretical results relative to this system appeared in several papers [1, 17, 18] and results about $^{36}Ar+$ ^{27}Al obtained with the Landau-Vlasov equation will be published separately [19].

The experimental set-up, the selection of well characterized events and their sorting as a function of the impact parameter are briefly described in sections 2 and 3, respectively (these two sections may be skipped if one has read [20]). Information obtained without determining the reaction plane is given in sections 4 (signature of fast emitted particles

2

at mid-rapidity) and 5 (determination of the energy of vanishing flow and the energy of uniform azimuthal distribution). A comparison of three methods used to determine the reaction plane is contained in section 6. Section 7 deals with the data relative to the flow parameter as a function of incident energy and impact parameter and the correction due to the error on the reaction plane determination. Data on azimuthal distributions are shown and discussed in section 8 while the conclusions are summarized in section 9.

2 Experimental set-up

The experiments were performed at the GANIL facility in the reaction chamber NAUTILUS. Charged products were detected in a nearly 4π geometry using two complementary multidetector systems MUR [21] and TONNEAU [22] (fig. 1 in ref. [20]).

The forward angles between 3.2° and 30° were covered by a wall of 96 plastic scintillators arranged in 7 concentric rings located 210 cm from the target. Angles between 30° and 150° were covered by a spherical barrel which was located 80 cm from the target.

The main improvements relative to ref. [16] (^{40}Ar+ ^{27}Al system) were the coverage from 90° to 150° and the addition of 7 large solid angle silicon telescopes installed 60 cm from the target and covering polar angles from 3° to 30° and an azimuthal range of 22°. These telescopes detected fragments with charges ≥ 3.

The overall geometrical efficiency of the array was 80 %. A positive high voltage of 45 kV was applied to the target in order to reduce electron emission. For the same purpose, aluminum foils 100 μm thick covered the scintillators. Due to these foils, only protons and α-particles having velocities above 2.48 cm/ns (3.2 MeV/u) were detected. This detection threshold increases with the charge, reaching 3.67 cm/ns (7.0 MeV/u) for ^{16}O.

For MUR and TONNEAU the velocities of particles and fragments were measured and the corresponding charges identified up to Z=9 using the energy-loss versus time-of-flight technique. For the telescopes, kinetic energies and charges were derived from a ΔE-E measurement. The masses of the fragments were estimated from their charges. Since kinematic analysis relies on velocities, the Si telescopes were accurately calibrated by means of fragments with Z ranging from 1 to 10 and velocities selected by a high resolution magnetic spectrometer in a separate measurement.

Two triggers have been used. The minimum bias trigger is called multiplicity trigger since any event where two detectors fired was recorded. The telescope trigger required detection by a telescope. Its purpose was to better study the peripheral events in which the projectile residue had a charge greater than 8 (limit of MUR and TONNEAU). We selected those events in which the heaviest fragment was detected in a telescope. In central and semi-central collisions, the charge of this fragment was found not to exceed 9, i.e. the multiplicity trigger events did not suffer from the scintillator limitation for charge identification. The results shown here have been obtained with the telescope trigger, and checked with the multiplicity trigger for central and semi-central collisions.

3

3 Sorting of events

3.a) Selection of well characterized events

The first step in the analysis was to select the events in which sufficient information was collected. This was achieved by requiring that the measured total parallel momentum $P_{//}$ be above 60% of the projectile linear momentum.

Indeed, contour levels of the correlation between $P_{//}$ / P_{proj} and the measured charged products multiplicity exhibit two hills [20]. One is located at $P_{//}$ / $P_{proj} = 0.8$ and corresponds to the average efficiency of the array. The other hill is located at low $P_{//}$ / P_{proj} values and small multiplicities. It corresponds to peripheral events in which the projectile-like fragment was emitted in a dead area or, mostly, below $3°$ (the grazing angle was $\sim 1°$). A cut at $P_{//}$ /$P_{proj} = 0.6$ eliminates such events. The importance of selecting well characterized events to get reliable data was shown in [20].

3.b) Impact parameter sorting

Since the directed collective flow depends on the violence of the collision, the next step was to sort the events as a function of the impact parameter. Actually, one uses a global variable which is sensitive to the violence of the collision, and the most violent collisions are attributed to head-on collisions.

The choice of global variables best suited to experiments on nucleus-nucleus collisions up to ~ 100 MeV/u was discussed in [23]. They were found to be the variables which make use of all detected products : the average (mass weighted) parallel velocity V_{av} (which takes advantage of the detection threshold) :

$$V_{av} = \frac{\sum_{i=1}^{\nu} \gamma_i m_i V_i cos\theta_i}{\sum_{i=1}^{\nu} \gamma_i m_i} \qquad (1)$$

and the sum of transverse momenta:

$$P_{\perp} = \sum_{i=1}^{\nu} |\overrightarrow{p_{ti}}| = \sum_{i=1}^{\nu} \gamma_i m_i V_i sin\theta_i \qquad (2)$$

where ν is the multiplicity of the event, m_i, V_i and θ_i are respectively the mass, velocity and polar angle of particle i, and p_{ti} its transverse momentum. Here γ_i is the usual relativistic coefficient .

The events were sorted in $P_{\perp}$ (or V_{av}) bins at all incident energies. Assuming a geometrical correspondance between $P_{\perp}$ (or V_{av}) and the impact parameter, the cross section of each bin can be expressed as an experimentally determined impact parameter, b_{exp} : the differential cross section $d\sigma/d(global\ variable)$ was obtained and integrated to get b_{exp} ($\sigma = \pi b_{exp}^2$). The advantage of this method is it does not require an accurate

4

measurement of the total reaction cross section which is difficult with charged particle detector arrays, since in peripheral reactions the quasi-projectile and quasi-target de-excite via neutron emission. The correlation between b_{exp} and the true impact parameter b has a FWHM of 1-2 fm [23].

The correlation between the values of b_{exp} obtained by V_{av} and $P_\perp$ respectively, for the same events corresponds to the correlation b_{exp} -b quoted above. Since V_{av} and $P_\perp$ are largely uncorrelated one can check whether they give the same sortings. Comparison between the data obtained with V_{av} and $P_\perp$ sortings are given in section 7, (fig. 10 and 11).

4 Signature of prompt emission at mid-rapidity

Let us first examine which information can be obtained without determining the reaction plane direction. An overall picture of the reactions is given by the bidimensional plots of the Lorentz invariant cross section versus the rapidity and the transverse momentum of the detected particles. Since several such plots were shown in [20] for the same system, only a few examples at 95 MeV/u are displayed in fig. 1.

The abcissa is the rapidity normalized to the beam rapidity in the laboratory, Y_r . This relative rapidity will be used on all figures in this paper, since it allows easier comparisons between different incident energies: the target rapidity is 0, the projectile rapidity is 1, the mid-rapidity is 0.5, the center-of-mass rapidity is very close to 0.57. The ordinate is the transverse momentum (i.e. the transverse rapidity) also normalized to the projectile rapidity.

The velocity thresholds and the angular limits of 3° and 150° are clearly seen. The low values of the threshold and minimum detection angle make it possible to see the emissions from a fast source (excited projectile-like) and a slow source (excited target-like) [20]. For this system at these energies, it was shown that binary dissipative processes (after pre-equilibrium emission) dominate even in central collisions [20, 24]. At mid-rapidity an excess of particles on Z=1 and Z=2 maps, especially in central collisions, can be attributed to prompt emission of the participant zone. The process is very close to deep inelastic transfer known at low energy (but accompanied by mid-rapidity emission) and to participant-spectator regime at high energy (but with a small number of emitted participants and a large excitation energy of the "spectators").

A difference between mid-rapidity particles and those emitted by the quasi-projectile and the quasi-target can be seen in their average transverse momentum per nucleon, $< p_t/A >$, displayed in fig. 2-a for three impact parameter bins for Z=1 particles (mostly protons). Fig. 2-b shows the same data for Z=2 particles (mostly α-particles). The solid line corresponds to the rapidity distribution dN/dY . Since velocities are measured, momenta per nucleon are directly obtained even without knowing the masses of the particles. The bump of the $< p_t/A >$ distribution around $Y_r = 0$ is due to the detection threshold

5

·(see fig. 1). Would there be only particles emitted by the "spectators", there would be a minimum at mid-rapidity in the $< p_t/A >$ distribution. On the contrary a maximum shows up clearly at 95 MeV/u. At 55 MeV/u it is less visible, due to the threshold effect which extends further in Y_r and to the smaller number of mid-rapidity particles emitted at this lower energy.

In order to check the shape of those distributions in the absence of prompt mid-rapidity emission, a simulation assuming two excited nuclei without pre-equilibrium emission for a very close system Ar + Ar at 74 MeV/u has been performed. The results are displayed in fig. 3. The closed circles correspond to the $< p_t/A >$ distributions and the solid lines to the dN/dY distributions. The distributions for Z=1 (left) and Z=2 (right) at three impact parameters are shown. As mentionned above, no mid-rapidity bump in $< p_t/A >$ distributions is seen even for central collisions, and a minimum is seen for the most peripheral reactions. This shows that the emissions from the two "spectators" cannot explain the bump observed in experimental data. It can be seen on rapidity distributions that evaporated Z=1 particles reach the mid-rapidity zone at all impact parameters. For Z=2 particles, this trend is observed for the most central collisions. This means that mid-rapidity particles are not only emitted in the first steps of the collision, but contain also particles evaporated from the "spectators". This feature was already observed in theoretical calculations [25, 19].

Two features characterize fig. 2-a and 2-b : i) the value of $< p_t/A >$ at mid-rapidity is independent of the impact parameter, ii) it is proportional to the projectile initial momentum for Z=1 particles (mostly protons) and almost proportional for Z=2. Both features are consistent with the following scenarii: 1) emission via collisions of projectile nucleons on target nucleons; 2) prompt emission from a neck between the "spectators" [26]; 3) prompt emission from the "spectators" just after separation. In [19], it was shown that most mid-rapidity particles are emitted in the first 60 fm/c after contact of the two colliding nuclei. Fig. 3 in [19] exhibits also a broad rapidity distribution of promptly emitted particles around mid-rapidity. The quasi-projectile and quasi-target rapidity zones receive significant contributions of those promptly emitted particles. Actually, the mixing of promptly emitted particles and evaporated particles is effective in the whole range of rapidities. In all cases, these promptly emitted particles are sensitive to the Coulomb field of the quasi-projectile and the quasi-target, which are close from each other at this stage of the collision. For such an almost symmetric system, it is difficult to separate the different contributions since the nucleon-nucleon frame rapidity Y_{nn} (corresponding to $Y_r =0.5$) and and the center-of-mass frame rapidity Y_{cm} are close to each other. In scenario 1, the emission should be centered at mid-rapidity whereas it should be centered close to center of mass rapidity in scenarii 2 and 3. We use the name of mid-rapidity emission because it is usual. That not does mean we exclude any scenario.

$< p_t/A >$ values are lower for Z=2 than for Z=1 at all rapidities. Around the quasi-projectile rapidity, thermal emission gives the same kinetic energy distribution above the

barrier to all emitted particles, i.e. a smaller energy per nucleon to clusters than to single nucleons. At mid-rapidity, the mechanism of formation of clusters must be understood in order to explain this feature.

For fig. 2-a and 2-b, the impact parameter sorting was made with the global variable V_{av}. Indeed the global variable used for impact parameter sorting should be uncorrelated, or at least weakly correlated, with the variable studied as a function of the impact parameter. This is the case for V_{av}, which uses only the longitudinal component of the velocity, weakly correlated with the transverse component. Conversely $P_\perp$ is strongly correlated with the values of p_{ti} (eq. 2). As a result, the dashed lines in fig. 4 obtained with $P_\perp$ show an increase of $< p_t >$ from peripheral collisions (low $P_\perp$ values) to central collisions (high $P_\perp$ values). They do however exhibit the same shapes as the solid lines obtained with V_{av}, and show the same signature of prompt mis-rapidity emission.

5 Azimuthal correlations

Another analysis which does not require to determine the reaction plane is the study of azimuthal correlations [14, 15]. They provide some features of collective motion and make it possible to obtain the values of the energy of vanishing flow (E_{bal}). The energy of uniform azimuthal distribution at mid-rapidity (E_{uni}) has been studied in [11].

The azimuthal correlation function $C(\Delta\phi)$ is defined if [15]. Typical azimuthal correlation functions are shown in fig. 5 at 67 MeV/u for three intervals of b_{exp} and for two intervals of Y_r . All type of particles have been considered together to construct $C(\Delta\phi)$. Other examples of correlation functions for 55, 86 and 95 MeV/u can be found in [15].

As shown in [14, 15], the azimuthal correlation of particles emitted above, or below, mid-rapidity is depending on the flow angle, and is characterized by a parameter λ_1. λ_1 is directly related to the 0°-180° asymmetry of the azimuthal correlation function $C(\Delta\phi)$:

$$\lambda_1 = \frac{C(0°) - C(180°)}{C(0°) + C(180°)} \qquad (3)$$

λ_1 reaches its minimum value at zero flow and increases both for positive and for negative flow [15]. The variations of λ_1 versus energy for Ar + Al reactions have been published in [15]. The extracted E_{bal} values are shown in fig. 10 of this reference together with data obtained from analysis based on reaction plane determination. For central collisions, the values of E_{bal} obtained with this method is 62 MeV/u for Zn + Ni, 66 MeV/u for Zn + Ti and 86 MeV/u for Ar + Al [15]. These values are consistent with the systematics shown in [6].

6 Reaction plane determination

6.a) Three methods

Several methods have been developped for determining the direction of the reaction plane. We want to compare three of them and determine which one(s) is (are) the best suited to our case. These methods are based on the sphericity tensor [27], the transverse momentum analysis [4] and the azimuthal correlation [28]. One can think also of using the direction of the projectile-like fragment but it was shown in [10] that this is a very rough approximation and cannot be used.

The three methods use the momenta associated with the detected particles. Since the total detected mass is not extremely large compared to the mass of each detected particle, an auto-correlation will appear if, for the determination of the reaction plane, one uses the particle whose direction relative to the reaction plane is studied. In order to avoid this auto-correlation, this particle is excluded from the reaction plane determination, which means that different reaction planes are obtained for all particles in an event.

One does not know on which side of the target nucleus the projectile was before the collision. Therefore one cannot determine if the particles deflected around the flow angle at forward angles are issued from the same side (positive flow) or the other side (negative flow). One obtains only the absolute value of the flow angle or of the flow parameter.

The sphericity tensor method was designed to fit the distribution of promptly emitted particles by a spheroid. For symmetry reasons, the direction of its main axis is in the reaction plane. When "spectator" particles are correctly eliminated, its angle relative to the beam axis is the absolute value of the flow angles [8]. This was not the case here, all detected particles were used and the largest axis direction determined only the reaction plane.

The transverse momentum analysis method uses the conservation of the initial transverse momentum : the sum of the transverse momentum projections in a plane for particles with rapidity above the center-of-mass rapidity Y_{cm} is equal and opposed to the sum for particles with rapidities below Y_{cm} . Since the collective flow of pre-equilibrium particles and bounce-off of spectators [29] deviate nucleons in the reaction plane direction, each sum is maximum when the projection plane is the reaction plane (see fig. 1). The estimated reaction plane of particle i is the plane containing the beam axis and the vector $\overrightarrow{Q_i}$ defined as :

$$\overrightarrow{Q_i} = \sum_{j=1, j \neq i}^{\nu} \omega_j (\overrightarrow{p_{tj}} + m_j \overrightarrow{V_i^b}) \qquad (4)$$

The meaning of the variables in this equation is the same as in eq. (1) and (2). The weight factor, ω_j , must have opposite signs for particles with $Y_r > Y_{rcm}$ and $Y_r < Y_{rcm}$. The convention defined in [4] is $\omega_j > 0$ for $Y_r > Y_{rcm}$ in order to get the absolute value

of the flow parameter. The exclusion of particle i from the sum (to avoid autocorrelation effects) means the total transverse momentum is no longer zero : it is $-p_{ti}$. To compensate for this effect, a recoil velocity correction is included in eq. (4), i.e. a velocity boost is applied to each particle j [29] :

$$\overrightarrow{V_i^b} = \frac{\overrightarrow{p_{ti}}}{M_{tot} - m_i} \qquad (5)$$

M_{tot} should be the total mass of the system. Since momentum conservation is applied to the detected particles, it can be also the total detected mass in the event. These different prescriptions have been tried. Their effect is to shift up or down the curves $<p^{x'}>(Y_r)$ without modifying noticeably their slopes at mid-rapidity (fig. 7-9). Since only these slopes are used to get the value of the flow parameter, there is no need to discuss this point further.

As recalled in section 1, at low incident energies the azimuthal distributions exhibit an in-plane enhancement. This correlation has been used [28] to determine the reaction plane. Instead of maximizing the projections of p_{tj} on the reaction plane as in the transverse momentum analysis (eq. 4), one minimizes the sum of the squared projections on the direction perpendicular to the reaction plane . A limitation of this method is that it does not say in which direction the particles with $Y > Y_{cm}$ are emitted; this is obtained via the transverse momentum analysis. Another limitation is that in-plane enhancement is required. In the case of uniform azimuthal distributions, the reaction plane is undetermined; in the case of out-of-plane enhancement (squeeze-out), it can be wrong by $90°$.

6.b)   Comparison of the methods

These methods can be compared via calculations based on simulation of nuclear reactions, but the conclusion will depend on the physical inputs. For instance, a large flow and a large deflection angle of the quasi-projectile will favor the first two methods, a strong in-plane enhancement will favor the third one. Therefore we compared the three methods on the data of this experiment.

A first hint is given by the angular dispersion of the reaction plane directions in the same event (since there are as many planes as detected particles). The dispersion between each plane and the average direction in the same event has been studied as a function of incident energy, impact and rapidity interval parameter. Gaussian distributions centered at $0°$ are observed with a variance ranging from $20°$ to $40°$, i.e. the distributions are narrow and are very close to each other with the sphericity tensor and transverse momentum methods. They are systematically larger with the azimuthal correlation method.

Another comparison is given by the angular differences between the directions given by two methods for the same particle, again as a function of incident energy, b_{exp} and

Y_r intervals. An example is shown in fig. 6. Clearly, the first and second methods give close directions. Again the third one often leads to a much more different direction.

The third method might in principle be better suited than the transverse momentum analysis method to the cases of zero or very weak flow values and in-plane enhancement [28]. Therefore the transverse analysis and azimuthal methods have been systematically tried. The transverse analysis method systematically gave larger values of flow parameters and in-plane enhancement factors, which means the error on the reaction plane determination was smaller with this method. All data shown hereafter have been obtained with this method.

7 In-plane component of the directed flow

The reaction plane being defined, the component of $\overrightarrow{p_t}$ of a particle on the reaction plane is $p^{x'}$ and the component perpendicular to this plane is $p^{y'}$, with the same notations as in [4, 10, 16]. Here (') means that these quantities are experimentally determined quantities subject to some error due to the reaction plane determination. For easier comparisons we will always consider $p^{x'}$ and p_t per nucleon.

At each Y_r value, there is a broad distribution of $p^{x'}/A$ and $p^{y'}/A$ values : the FWHM is in the range 150-250 MeV/c per nucleon [10]. Since one is interested in variations of $<p^{x'}/A>$ versus Y_r an order of magnitude lower than this FWHM, one should make sure there is no dependence due to the set-up and/or the calibration procedure. For this purpose, instead of using the reaction plane, a fixed plane was randomly chosen and the variation of $<p^{x'}/A>$ and $<p^{y'}/A>$ relative to this plane were plotted. This method is a sensitive way of checking the whole calibration chain. The values of $<p^{x'}/A>$ and $<p^{y'}/A>$ first showed small bumps at some rapidities. This was found to be due to some small mistakes in reporting calibration parameters. After correction, $<p^{x'}/A>$ and $<p^{y'}/A>$ exhibited no systematic variation with Y_r and stayed close to zero (within ± 5 MeV/c per nucleon in the range $Y_r =0\text{-}1$). Projections on the reaction plane could then be studied.

7.a) Flow parameter F

Fig. 7 shows the variation of $<p^{x'}/A>$ versus Y_r for charge 1 particles (mostly protons) in six impact parameter bins at 55 MeV/u (lowest energy). Fig. 8 and fig. 9 show similar distributions for Z=2 particles at 55 MeV/u and 86 MeV/u respectively. In addition, the results obtained with the two impact parameter sortings are shown in fig. 8. They are very similar.

Due to total transverse momentum conservation, the value of $<p^{x'}/A>$ should be zero at Y_{rcm}. As said above, this value is sensitive to the value of M_{tot} in eq. 4. Here M_{tot} was taken as the total detected mass, which leads to the correct value $<p^{x'}/A>$ at

10

Y_{rcm} in central and semi-central collisions, but to negative values in peripheral collisions. Conversely the use of the total system mass leads to $<p^{x'}/A> = 0$ in peripheral collisions (not shown here) and positive values in central and semi-central collisions, but the slope at mid-rapidity is unchanged.

Since relative rapidities are used, this slope is the in-plane (or sidewards) flow parameter value, F. It is determined by a linear fit shown as straight lines in the figures.

In peripheral collisions the rapidities of the "spectator" sources are close to 0 and 1 (see fig. 2) and the linear variation, characteristics of oriented collective motion, is observed on a broad range of Y_r values. Conversely in central collisions, the "spectator" sources come closer to mid-rapidity and leave the collective flow behaviour unperturbed on a narrower range.

7.b) Measured versus real flow values

As said above, there is some error in determining the reaction plane direction. For one particle in an event, the angle between the real and estimated direction is called θ. θ is not known for each particle and event, but its average value on many events can be estimated by making some assumptions on the origin of the correlations between the particles in an event. A correction factor $1/cos < \theta >$ can be applied to the data [4, 30].

This deviation is mostly due to the finite number of detected nucleons and to the randomly oriented thermal motion superimposed to the collective momentum. When the collective momentum is large, one obtains a good location of the reaction plane. In the opposite case, the alignment due to the collective momentum is washed out by the thermal motion and the reaction plane determination is subject to a large error. The experimental limitations increase this error, but simulation calculations have shown that they play a minor role with the 4π array used here [12].

Formulae [4, 30] and simulations [12] have been used to estimate the correction factor to be applied to the data. Since some hypotheses are made in these formulae and simulations, the correction factor itself is subject to some uncertainty. When the flow is large, the factor is not much greater than 1 and its own uncertainty is not large. But when the flow has small values as here, the correction factor becomes much larger than 1 and is poorly defined.

Actually the most meaningful procedure is to keep the raw experimental data and introduce the error on the reaction plane determination in the theoretical study. This procedure was used in [19]. If one wants nevertheless to estimate the correction factor in experimental data, simulation calculations have shown that the method described in [30] gives the most realistic values for the system studied here. The correction factors extracted from the study performed in [19] lead to the same conclusion. This formula has been modified to take into account the recoil due to the particle excluded from the reaction plane determination [31]. Some corrected data are shown in fig. 12 together with

11

uncorrected values.

7.c) Dependence of F on the impact parameter

The uncorrected values of F obtained from the above analysis are plotted in fig. 10 as a function of the impact parameter b_{exp} for the five energies investigated. b_{exp} has been obtained with the V_{av} sorting. F must be zero for head-on collisions (b=0) for symmetry reasons and increases with b_{exp} in central and semi-central collisions. Weak values are indeed observed for the most central b_{exp} bin. F should be zero again for grazing collisions. Here $b_{grazing} \approx 8$ fm. No data can be obtained above 7 fm, but a decrease of F with increasing b_{exp} is observed above ~ 5 fm.

At each energy, F is larger for Z=2 than for Z=1. That has been attributed to thermal energy effects. The thermal moment of a particle is randomly oriented and tends to destroy the in-plane alignment due to the collective flow. The average thermal energy is the same whatever the mass A of the particle, so the thermal momentum *per nucleon* varies as $A^{-1/2}$ and is smaller for heavier particles. This effect was observed for high energies (positive flow) [8] and comes out in several theoretical studies at high energies [32, 33] and at low energies [19]. At low energies (negative flow) it can also be explained as due to the presence of two components of flow [25, 35].

The influence of the impact parameter sorting can be seen in fig. 11 which shows the results obtained with the $P_\perp$ sorting. To facilitate the comparison with fig. 10, identical scales have been used. One observes an overall agreement with fig. 10 and some differences. Slightly larger value of F for Z=2 are observed at the highest incident energies. The main differences are observed for large values of b_{exp} . Therefore we will not use values of F obtained for $b_{exp} > 6$ fm .

7.d) Dependence of flow on the incident energy

Fig. 12 shows the dependence on the incident energy of F for Z = 1 and Z = 2 and for two impact parameters : $b_{exp} \leq 2.5$ fm and 5 fm $< b_{exp} < 5.5$ fm . In addition to the uncorrected F values, values corrected for the uncertainties affecting the reaction plane determination are plotted.

As only the absolute value of F can be determined in the experiment, at the lowest measured energy a negative sign has been ascribed to the flow parameter, in agreement with theoretical calculations. At other energies the sign of the flow is determined by continuity.

The data obtained previously for collisions $^{36}Ar+^{27}Al$ from 35 to 85 MeV/u are also shown. They agree with the present data within experimental errors. One can see from this figure that E_{bal} is around 90 MeV/u and increases slowly with the impact parameters. This value is in agreement with the systematics shown in [6]. The flow parameters for Z = 2 participants are systematically larger (in absolute value) than for Z = 1. For Z=2,

12

in peripheral collisions, one can guess a slightly higher E_{bal} for Z $=2$ than for Z $= 1$, but since the sign of the flow parameters is not obtained experimentally, it is difficult to draw a definite conclusion. Would the sign of F for Z $=2$ at 95 MeV/u be positive, we would have practically the same values for Z $= 1$ and Z $= 2$. In central collisions, the data do not show a dependence of E_{bal} on Z.

8   Azimuthal distributions

Besides the sidewards flow, described by the flow parameter, other collective effects can be present in the spatial distribution of the participants [3, 8, 10]: i) squeeze-out effects, seen at higher energies and which could be a signature of shadowing by the spectators, resulting in a preferential emission perpendicular to the reaction plane [34]; ii) a rotation-like behaviour of the participant zone [9] which manifests itself by a preferential emission in the reaction plane.

In order to look for such collective effects the azimuthal distributions of particles with Z $= 1$ and Z $= 2$ have been studied. The azimuthal angle ϕ is the angle between the transverse momentum of the particle and the vector $\overrightarrow{Q}$ (equation 4) associated to the estimated reaction plane.

The polar axis used to build these azimuthal distributions is the beam direction. The disadvantage of using the beam direction is that the measured azimuthal anisotropy of midrapidity particles is partly due to the in-plane flow angle Θ_F . To avoid this coupling of in-plane flow to the azimuthal anisotropy, the authors of [36] used the flow axis as polar axis. At the bombarding energies used for our system the determination of Θ_F via the kinetic energy tensor analysis suffers for very large fluctuations due to the small number of emitted participants and to particles emitted by the "spectators", and to the impossibility to separate the particles evaporated by the "spectators" from promptly emitted particles.

In fig. 13, one can see as histograms the azimuthal distributions $dN/d\phi$ for Z $= 1$ particles at 55 MeV/u incident energy, for three bins in the relative rapidity Y_r and for three impact parameters. For Z $= 2$, the azimuthal distributions look similar.

Here, $\phi = 0°$ and $\phi = \pm 180°$ correspond to the reaction plane , and $\phi = \pm 90°$ means directions perpendicular to the reaction plane.

The azimuthal distributions are well described by the function :

$$\frac{dN}{d\phi} = a_0 + a_1 cos\phi + a_2 cos2\phi \qquad (6)$$

The variation of a_1/a_0 with rapidity is directly connected to the flow parameter [3]. a_2/a_0 is related to the other collective effects quoted at the beginning of this section. So, a positive value of a_2/a_0 corresponds to maxima at $\phi = 0°$ and $\phi = \pm 180°$ (that is, in the reaction plane), and thus to a rotation-like effect. A negative value of a_2/a_0 corresponds to maxima at $\phi = \pm 90°$ (that is, out-of-plane) and thus to a squeeze-out effect.

Detailed information has also been gained for the azimuthal distributions. An in-plane

The solid curves in fig. 13 show the results of a fit of equation (6) to the data. The dashed curves show the $a_1 cos\phi$ terms (shifted up for clarity) and the dotted curves show the anisotropy term $a_2 cos2\phi$ (shifted up).

For a definite impact parameter and for small rapidities ($Y_r = 0.0 - 0.2$) a_1 is negative in agreement with the fact that the particles moving backward in the CM system are preferentialy emitted in the reaction plane at $\phi \pm 180°$.

On the contrary, for rapidities close to the projectile rapidity ($Y_r = 0.8 -1$), a_1 is positive, which corresponds to a preferential emission in the reaction plane, at $\phi = 0$, for particles moving forward in the CM. For mid-rapidity particles ($Y_r = 0.4 - 0.6$) a_1 is close to zero. It should be zero, because here $< p^x/A >$ should be exactly zero. It deviates from zero, due to uncertainties related to the recoil corrections in the reconstruction of the reaction plane.

In the following we shall confine our discussion to the ratio a_2/a_0. Fig. 14 shows the evolution of a_2/a_0 on the impact parameter for mid-rapidity particles $Z = 1,2$ at each incident energy. a_2/a_0 is larger for $Z = 2$ particles than for $Z = 1$ particles. At low energies a clear increase of a_2/a_0 with the impact parameter is seen, in qualitative agreement with a rotation-like behaviour.

For a definite impact parameter a_2/a_0 decreases with the incident energy but remains always positive, suggesting a rotation of the participant zone at all energies, contrary to the system $^{64}Zn +^{58} Ni$ in the same energy range where a transition from rotation-like behaviour to squeeze-out was observed [11].

This rotation-like behaviour of mid-rapidity particles is reproduced by BUU calculations [18], and QMD calculation on a close system Ca + Ca [35].

9   Conclusions

A complete set of in-plane flow parameters values has been obtained for $^{36}Ar +^{27} Al$ system as a function of incident energy, impact parameter and charge of the emitted fragment. The inversion of the flow direction occurs at the upper limit of the incident energy range, i.e. around 90 MeV/u.

The energy of vanishing flow was also determined using a method which does not require the reconstruction of the reaction plane. The same values of E_{bal} have been obtained as those obtained with the transverse momentum analysis method.

The observed flow values are larger for heavier fragments. This is qualitatively attributed to the larger thermal energy per nucleon of lighter fragments, however a quantitative calculation is needed. Coulomb effects also play a role [6]. Another pending problem is the possible variation of the balance energy with the mass of the emitted fragment. The origin of mid-rapidity particles has to be fully understood to separate the contributions of the possible production mechanisms (evaporation from quasi-projectile and quasi-target, emission from a neck, nucleon-nucleon collisions).

Detailed information has also been gained for the azimuthal distributions. An in-plane enhancement is observed for this system at all energies studied, i.e. up to 95 MeV/u, but it decreases with energy.

Detailed comparisons with theoretical calculations have to be performed in order to get informations on the in-medium nucleon-nucleon interaction [6, 2]. Due to the complexity of the experimental set-up and of the analysis methods, it is difficult to correct the experimental results. Then, to obtain accurate values of the parameters of this interaction, the calculations have to be filtered by the experimental set-up and analyzed in the same way as the experimental events are, i.e. the sorting of events and the reaction plane determination procedures have to be performed on the theoretical calculations [19].

References

[1] F. Sébille, G. Royer, C. Gregoire, B. Remaud and P. Schuck,

Nucl. Phys, A501 (1989) 137

[2] Bao-An Li

Physical Review C48 (1993) 2415

[3] M. Demoulins, D. L'Hôte, J.P. Alard, J. Augerat, R. Babinet, N. Bastid, F. Brochard, C.Cavata, N. de Marco, P. Dupieux, H. Fanet, Z. Fodor, L. Fraysse, P. Gorodetzky, J. Gosset, T. Hayashino, M.C. Lemaire, A. Le Merdy, B. Lucas, J. Marroncle, G. Montarou, M.J. Parizet, J. Poitou, C. Racca, W. Schimmerling, Y. Terrien and O. Valette,

Physical Review Letters B241 (1990) 476

J. Gosset, M. Demoulins, D. L'Hôte,O. Valette, J.P. Alard, J. Augerat, R. Babinet, N.Bastid, F. Brochard, C.Cavata, P. Charmensat, N. de Marco, P. Dupieux, H. Fanet, Z.Fodor, L. Fraysse, P. Gorodetzky, M.C. Lemaire, B. Lucas, J. Marroncle, G. Montarou, M.J. Parizet, J. Poitou, D. Qassoud,C. Racca, A. Rahmani, W. Schimmerling, and Y. Terrien ,

Rapport DPhN/Saclay No. 2568 , 07/1989 and

Talk at Int. Advanced Courses on "The Nuclear Equation of State", Peniscola, (Spain), May, 1989.

[4] P. Danielewicz and G. Odyniec,

Physics Letters B157 (1985) 146

[5] S.C. Jeong et al. (FOPI collaboration)

Physical Review Letters, 72 (1994) 3470

[6] V. de la Mota, F. Sebille, M. Farine, B. Remaud and P. Schuck,

Physical Review C46 (1992) 677

[7] G.D. Westfall, W. Bauer, D. Craig, M. Cronqvist, E. Gaultieri, S. Hannuschke, D. Klakow, T. Li, T. Reposeur, A.M. Vander Molen, W.K. Wilson, J.S. Winfield, J. Yee, S.J. Yennello, R. Lacey, A. Elmaani, J. Lauret, A. Nadaser and E. Norbeck

Physical Review Letters 71 (1993) 1986

[8] H.H. Gutbrod, K.H. Kampert, B.W. Kolb, A.M. Poskanzer, H.G. Ritter and H.R. Schmidt,

Physics Letters B216 (1989) 267

[9] W.K. Wilson, W. Benenson, D.A. Cebra, J. Clayton, S. Howden, J. Karn, T. Li, C.A. Ogilvie, A. Vander Molen, G.D. Westfall, J.S. Winfield, B. Young and A. Nadasen,

Physical Review C41 (1990) R1881

[10] W.Q. Shen, J. Péter, G. Bizard, R. Brou, D. Cussol, M. Louvel, J.P. Patry, R. Regimbart, J.C. Steckmeyer, J.P. Sullivan, B. Tamain, E. Crema, H. Doubre, K. Hagel, G.M. Jin, A. Péghaire, F. Saint-Laurent, Y. Cassagnou, R. Legrain, C. Lebrun, E. Rosato, R. Mac Grath, S.C. Jeong, S.M. Lee, Y. Nagashima, T. Nakagawa, M. Ogihara, J. Kasagi and T. Motobayashi,

Nuclear Physics A551 (1993) 333

[11] R. Popescu, J.C. Angélique, A. Péghaire, G. Bizard, C. Auger, R. Brou, A. Buta, C.Cabot, Y. Cassagnou, E. Crema, D. Cussol, Y. El Masri, Ph. Eudes, M. Gonin, K. Hagel, Z.Y. He, A. Kerambrun, C. Lebrun, R. Legrain, J.P. Patry, J. Péter, R. Regimbart, E. Rosato, F. Saint-Laurent, J.C. Steckmeyer, B. Tamain, E. Vient and R. Wada,

Physics Letters B331 (1994) 285

[12] J.P. Sullivan and J. Péter,

Nuclear Physics A540 (1992) 275

[13] S. Wang, Y.Z. Jiang, Y.M. Liu, D. Keane, D. Beavis, S.Y. Chu, S.Y. Fung, M. Vient, C. Hartnack and H. Stöcker,

Physical Review C44 (1991) 1091

[14] R.A. Lacey, A. Elmaani, J. Lauret, T. Li, W. Bauer, D. Craig, M. Cronqvist, E. Gualtieri, S. Hannuschke, T. Reposeur, A. Vander Molen, G.D. Westfall, W.K. Wilson, T.S. Wienfield, J. Yee, S. Yennello, A. Nadasen, R.S. Tickle and E. Norbeck,

Physical Review Letters 70 (1993) 1224

[15] A. Buta, J.C. Angélique, C. Auger, G. Bizard, R. Brou, C.Cabot, Y. Cassagnou, E. Crema, D. Cussol, Y. El Masri, Ph. Eudes, M. Gonin, K. Hagel, Z.Y. He, A. Kerambrun, C. Lebrun, R. Legrain, J.P. Patry,A. Péghaire, J. Péter, R. Popescu, R. Regimbart, E. Rosato, F. Saint-Laurent,J.C. Steckmeyer, B. Tamain, E. Vient and R. Wada,

Nuclear Physics A584 (1995) 397

[16] J.P. Sullivan, J. Péter, D. Cussol, G. Bizard, R. Brou, M. Louvel, J.P. Patry, R. Regimbart, J.C. Steckmeyer, B. Tamain, E. Crema, H. Doubre, K. Hagel, G.M. Jin, A. Péghaire, F. Saint-Laurent, Y. Cassagnou, R. Legrain, C. Lebrun, E. Rosato, R.

Mc Grath, S.C. Jeong, S.M. Lee, Y. Nagashima, T. Nakagawa, M. Ogihara, J. Kasagi and T. Motobayashi,

Physics Letters B249 (1990) 8

[17] A. Ohnishi, T. Maruyama and H. Horiuchi,

Nuclear Physics A538 (1992) 429c

[18] Y.G. Ma, W.Q. Shen, J. Feng and Y.Q. Ma,

Zeitschrift für Physiks, A346 (1993) 285

Y.G. Ma and W.Q. Shen

Physical Review C51 (1995) 3256.

[19] Z.Basrak, P.Eudes, P.Abgrall, F.Haddad and F.Sébille

Rapport Interne SUBATECH 95-13

Submitted to Physical Review C

[20] J.Péter, S. C. Jeong, J.C. Angélique, G. Auger, G. Bizard, R. Brou, A. Buta, C.Cabot, Y. Cassagnou, E. Crema, D. Cussol, D.Durand, Y. El Masri, Ph. Eudes, Z.Y. He, A. Kerambrun, C. Lebrun, R. Legrain, J.P.Patry, A. Péghaire, J. Péter, R. Popescu, R. Régimbart, E. Rosato, F. Saint-Laurent, J.C. Steckmeyer, B. Tamain, and E. Vient ,

Nuclear Physics A593 (1995) 95

[21] G. Bizard, A. Drouet, F. Lefebvres, J.P. Patry, B. Tamain, F. Guilbault and C. Lebrun,

Nuclear Instruments & Methods A244 (1986) 483

[22] A. Péghaire, B. Zwieglinski, E. Rosato, G.M. Jin, J. Kasagi, H. Doubre, J. Péter, Y. Cassagnou, F. Guilbault, C. Lebrun and R. Legrain,

Nuclear Instruments & Methods A299 (1990) 365

[23] J. Péter, D. Cussol, G. Bizard, R. Brou, M. Louvel, J.P. Patry, R. Regimbart, J.C. Steckmeyer, J.P. Sullivan, B. Tamain, E. Crema, H. Doubre, K. Hagel, G.M. Jin; A. Péghaire, F. Saint-Laurent, Y. Cassagnou, R. Legrain, C. Lebrun, E. Rosato, R. Mc Grath, S.C. Jeong, S.M. Lee, Y. Nagashima, T. Nakagawa, M. Ogihara, J. Kasagi and T. Motobayashi,

Nuclear Physics A519 (1990) 611

[24] A. Kerambrun, J.C. Angélique, C. Auger, G. Bizard, R. Brou, A. Buta, C.Cabot, Y. Cassagnou, E. Crema, D. Cussol, Y. El Masri, Ph. Eudes, M. Gonin, K. Hagel,

18

Z.Y. He, S.C. Jeong, C. Lebrun, R. Legrain, A. Péghaire, J. Péter, R. Regimbart, E. Rosato, F. Saint-Laurent,J.C. Steckmeyer, B. Tamain, E. Vient and R. Wada,

LPCC 94-14, to be submitted to Zeitschrift für Physiks A

[25] A. Ono and H. Horiuchi,

Physical Review C51 (1995) 299

[26] D.E.Fields et al.,

Physical Review Letters 69 (1992) 3713

[27] M. Gyulassy, K.A. Frankel and H. Stöcker,

Physics Letters B110 (1982) 185

[28] M.K. Wilson, R. Lacey, C.A. Ogilvie and G.D. Westfall,

Physical Review C45 (1992) 738

[29] C.A. Ogilvie, D.A. Cebra, J. Clayton, P. Danielewicz , S. Howden, J. Karn, A. Nadasen, A. Vander Molen, G.D. Westfall, W.F. Wilson and J.S. Winfield,

Physical Review C40 (1990) 2592

[30] P. Danielewicz, H. Ströbele, G. Odyniec, D. Bangert, R. Bock, R. Brockmann, J.W. Harris, H.G. Pugh, W. Rauch, R.E. Renfordt, A. Sandoval D. Schall, L.S. Schoeder and R. Stock,

Physical Review C38 (1988) 120

[31] W.M.Zhang, R.Madey, M.Elaasar, J.Schambach, D.Keane, B.D.Anderson, A.R.Baldwin, J.Cogar, J.W.Watson, G.D.Westfall, G.Krebs, H.Wieman

Physical Review C42 (1990) R491

[32] S.Leray , C.Ngô, M.E.Spina, B.Remaud, F.Sébille

Nuclear Physics A511 (1990) 414

[33] V. Koch, B. Blättel, W. Cassing, U. Mosel and K. Weber,

Physics Letters B241 (1990) 174

[34] C.Hartnack et al., Nuclear Physics A538 (1992) 53c

[35] S.Soff, S.A.Bass, C.Hartnack, H.Stöcker, W.Greiner

Physical Review C51 (1995) 3320

[36] H.H.Gutbrod, K.H.Kampert, B.Kolb, A.M.Poskanzer, H.G.Ritter, R.Schicer, H.R.Schmidt

Phisical Review C42 (1990) 640
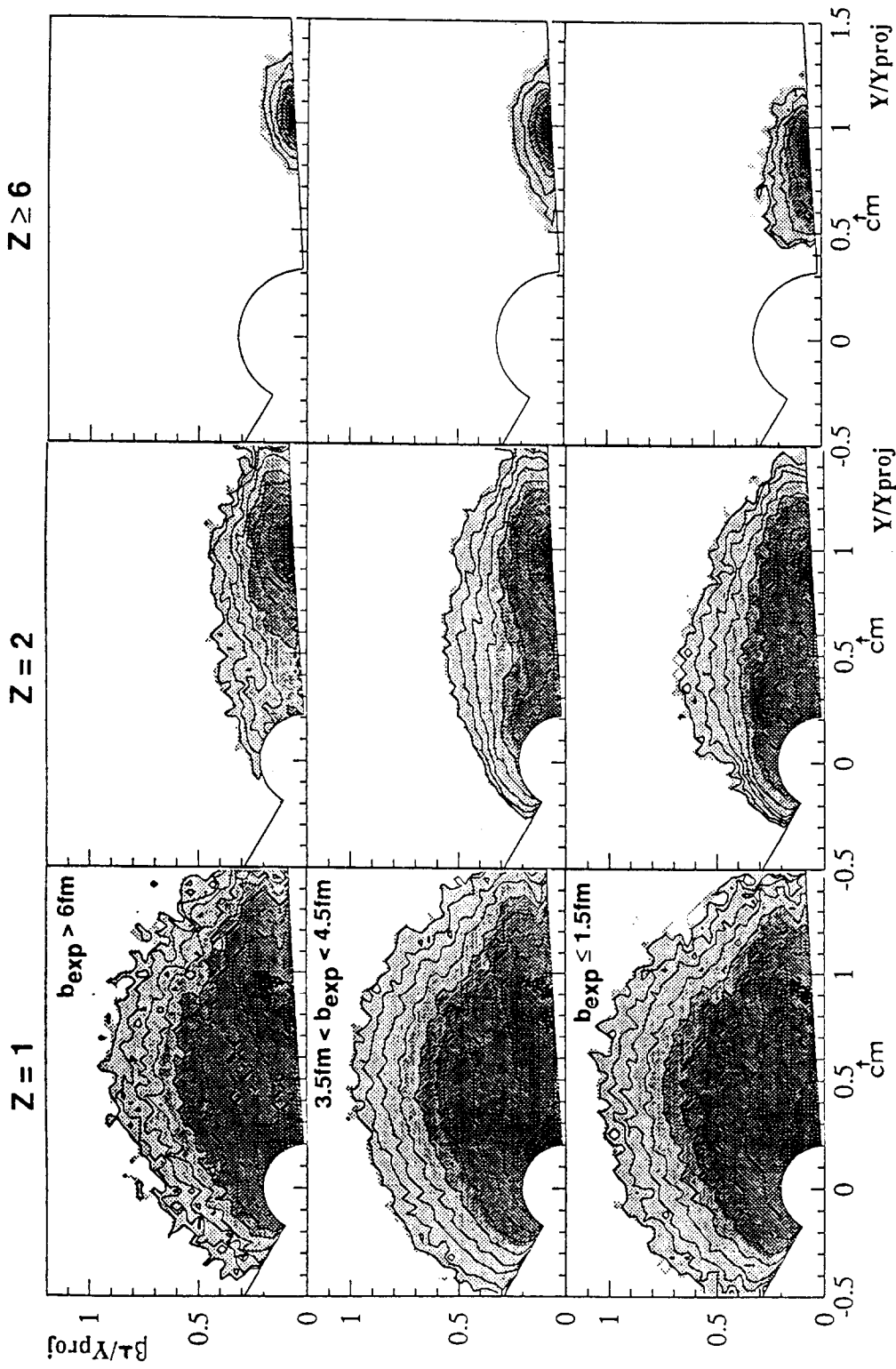
Figure 1: Invariant cross-sections, $\frac{d^2\sigma}{d\beta_\perp dy_r}$, for E=95 MeV incident energy, from central (higher row) and peripheral (lower row) events. Each column corresponds to a different type of particles.
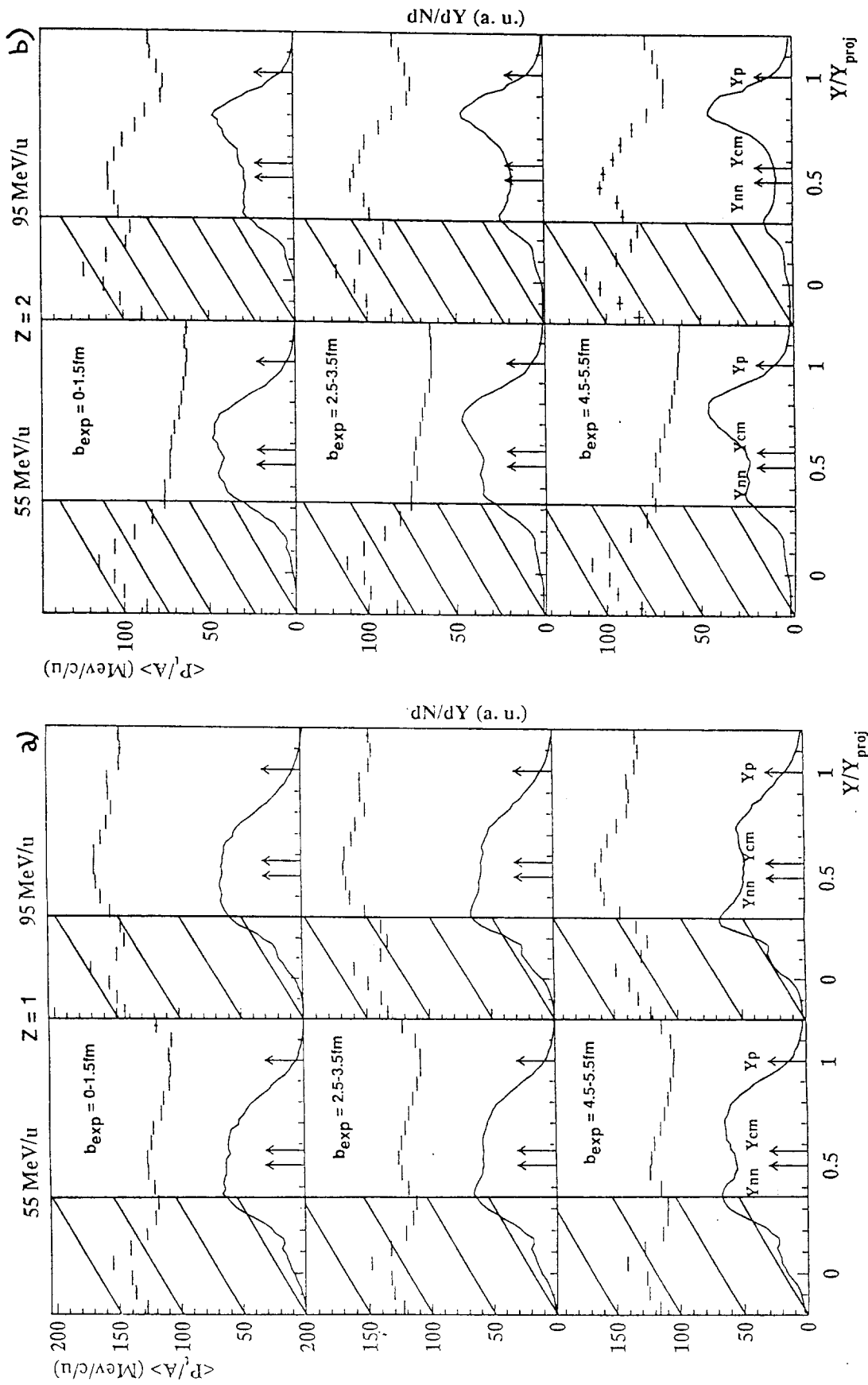
Figure 2: Average transverse momentum distributions versus rapidity for Z=1 particles (a), Z=2 particles (b), two incident energies and three experimentally estimated impact parameters. On each plot, the solid line corresponds to the rapidity distribution in arbitrary units.
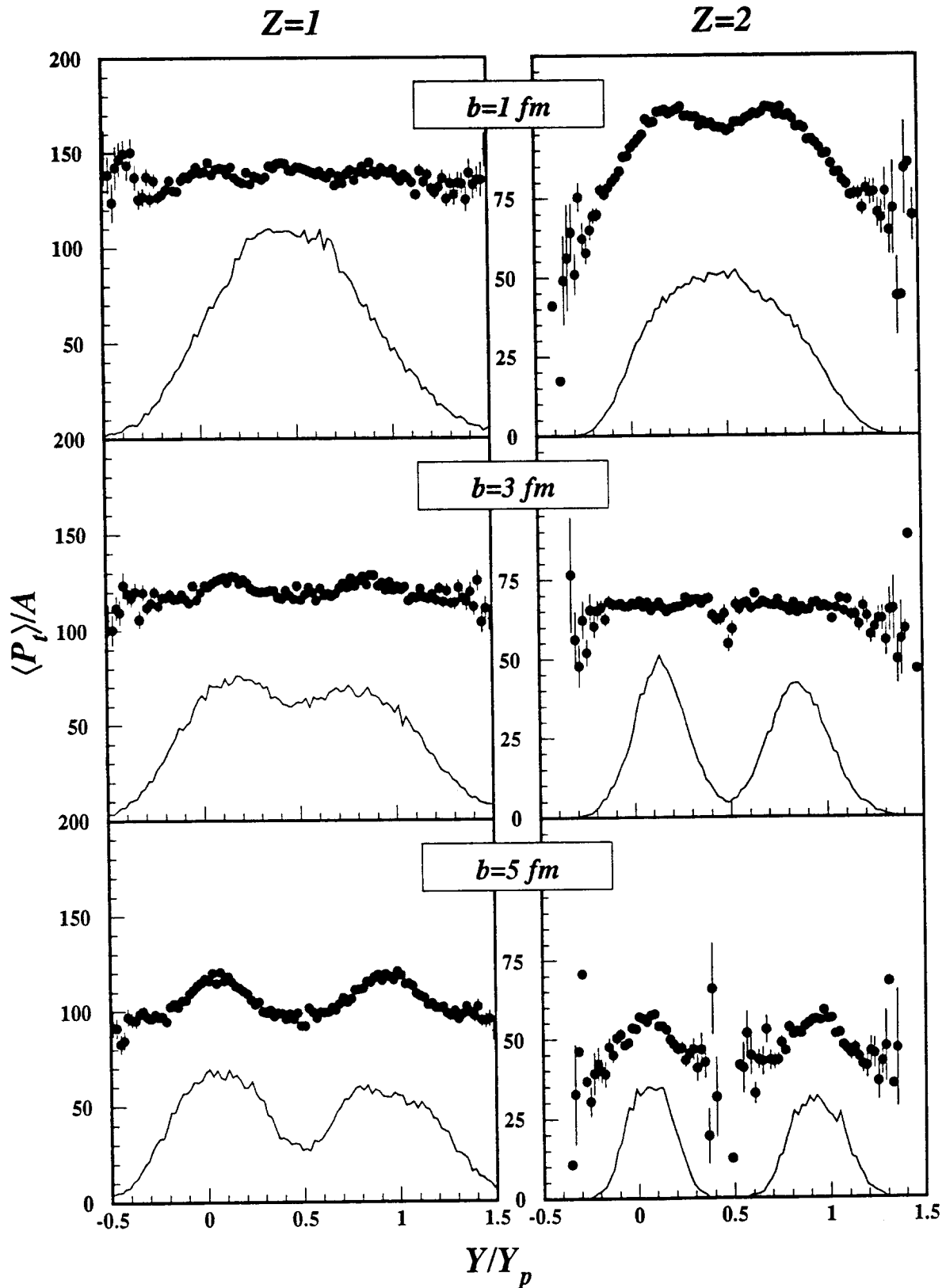
Figure 3: Average transverse momentum distributions versus rapidity obtained from a simulation assuming two excited nuclei without fast emission (see text), for Z=1 (right) and Z=2 particles (left) at three impact parameters. The solid line on each plot corresponds to the rapidity distribution in arbitrary units.
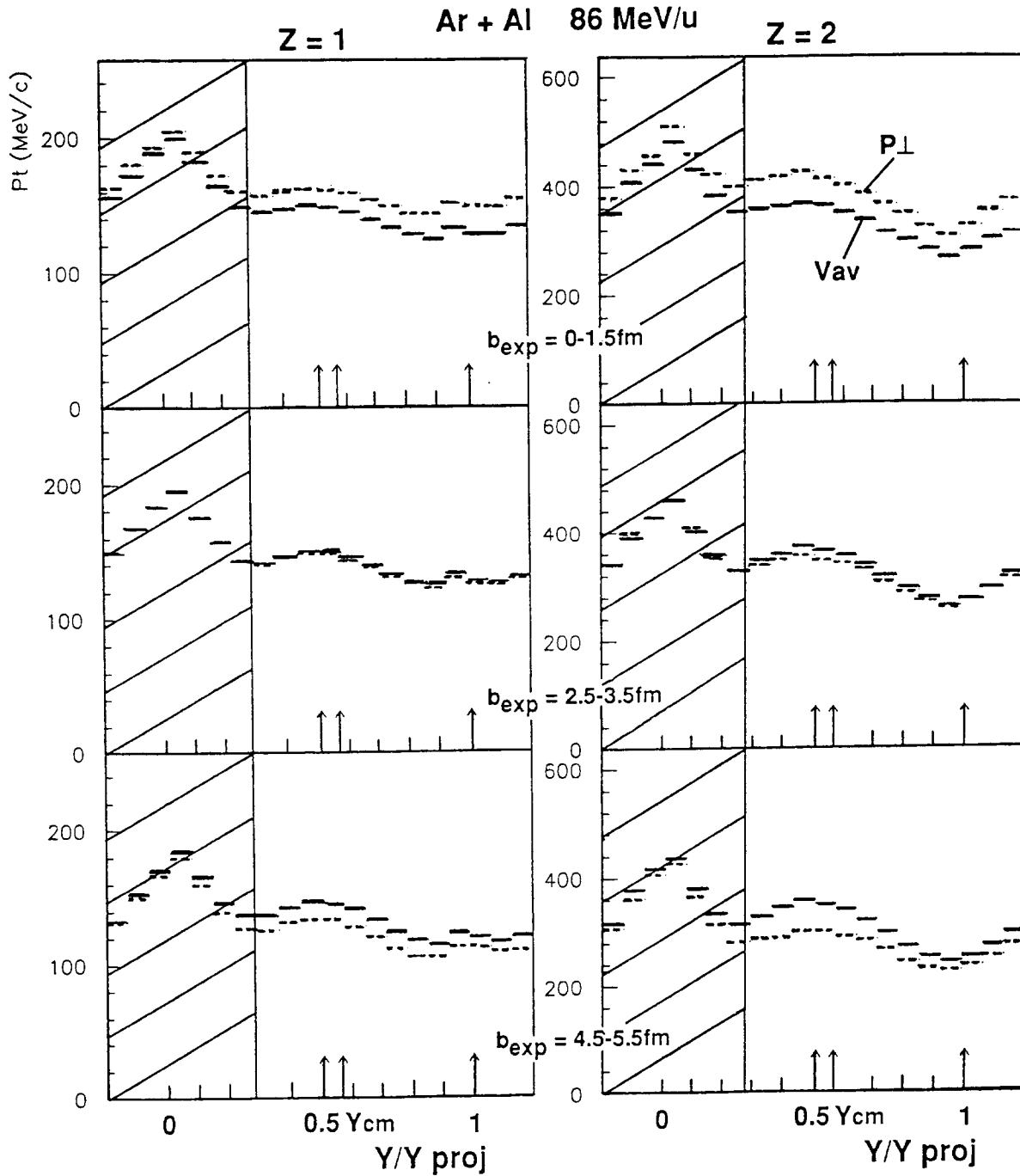
Figure 4: Average transverse momentum distributions versus rapidity for Z=1 (left) and Z=2 (right) particles at 86 MeV/u for three experimentally determined impact parameters. The solid lines correspond to the V_{av} sorting and the dashed lines correspond to the $P_{\perp}$ sorting (see text).
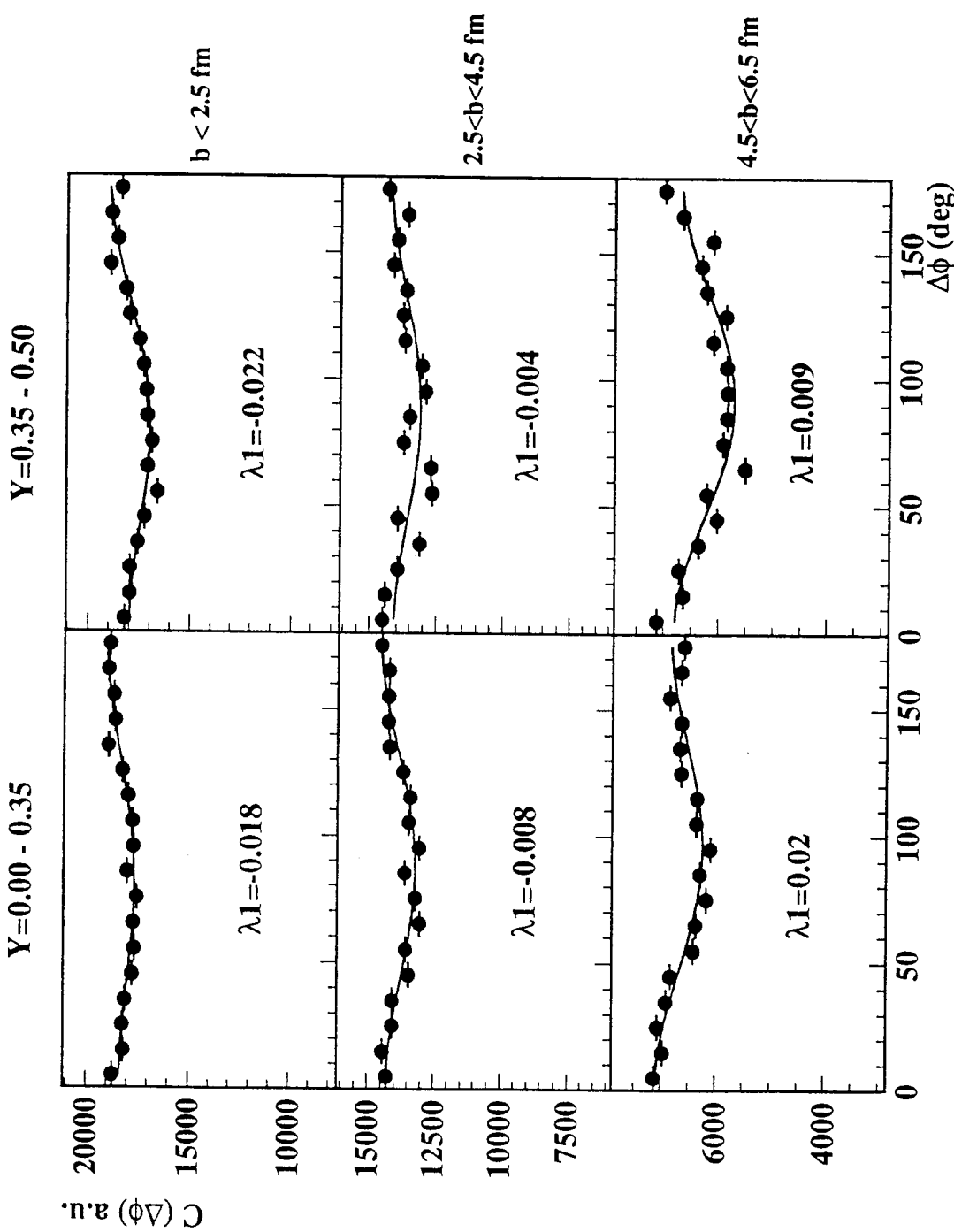
Figure 5: Experimental azimuthal correlation functions (full points), for E=67 MeV/u incident energy, two intervals of rapidity and three intervals of impact parameters. The solid line on each plot is a fit to the experimental data with the following expression $C(\Delta\phi) = A(1 + \lambda_1 cos\Delta\phi + \lambda_2 cos2\Delta\phi)$ where A, λ_1 and λ_2 are free parameters (see [15]).
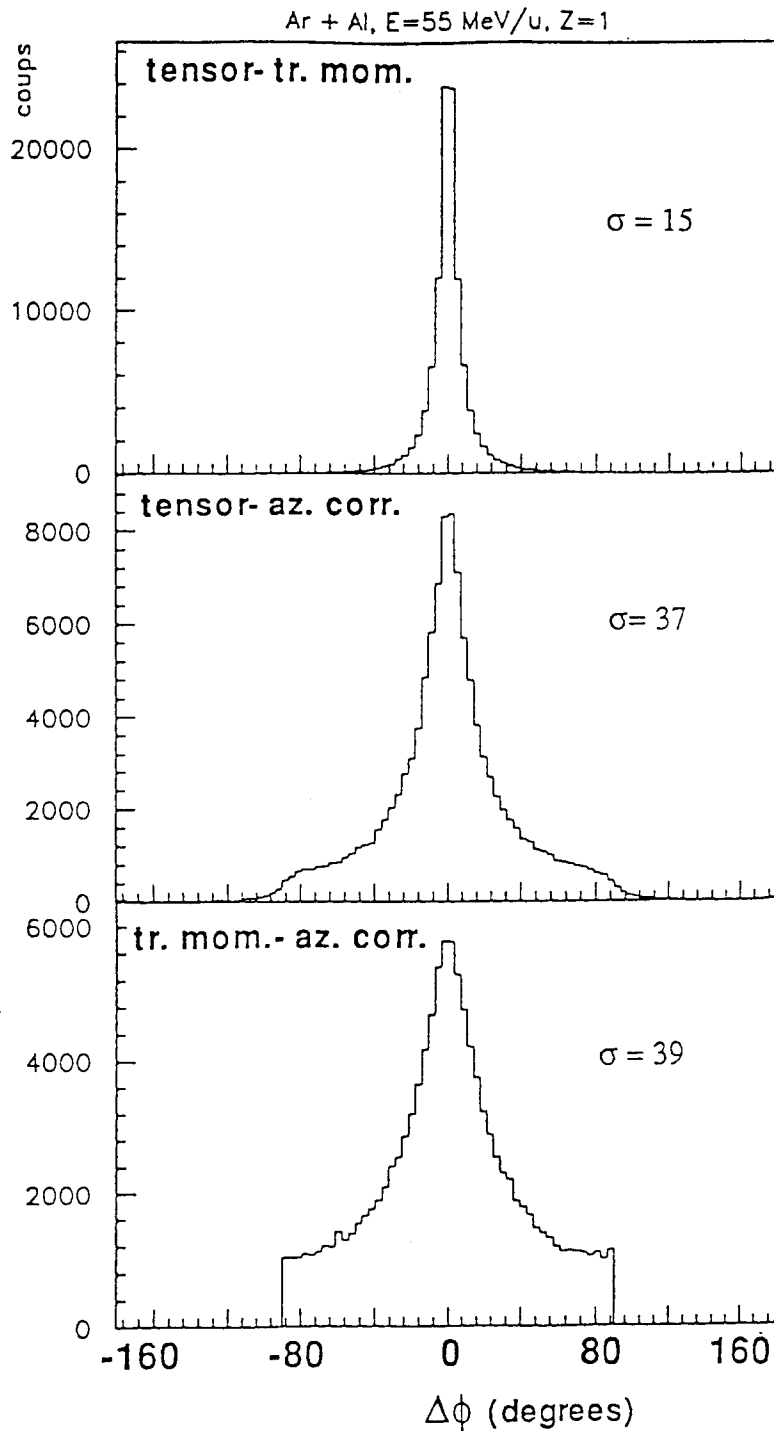
Figure 6: The distributions of the azimuthal angles between pairs of reaction planes determined for each particle using two different methods for the reaction plane reconstruction. The two compared methods, mentionned in each pannel are explained in the text. The distributions refer to E=55 MeV/u, mid-rapidity Z=1 particles and an impact parameter $b_{exp} \approx 3$ fm. Here σ is the variance of each distribution.
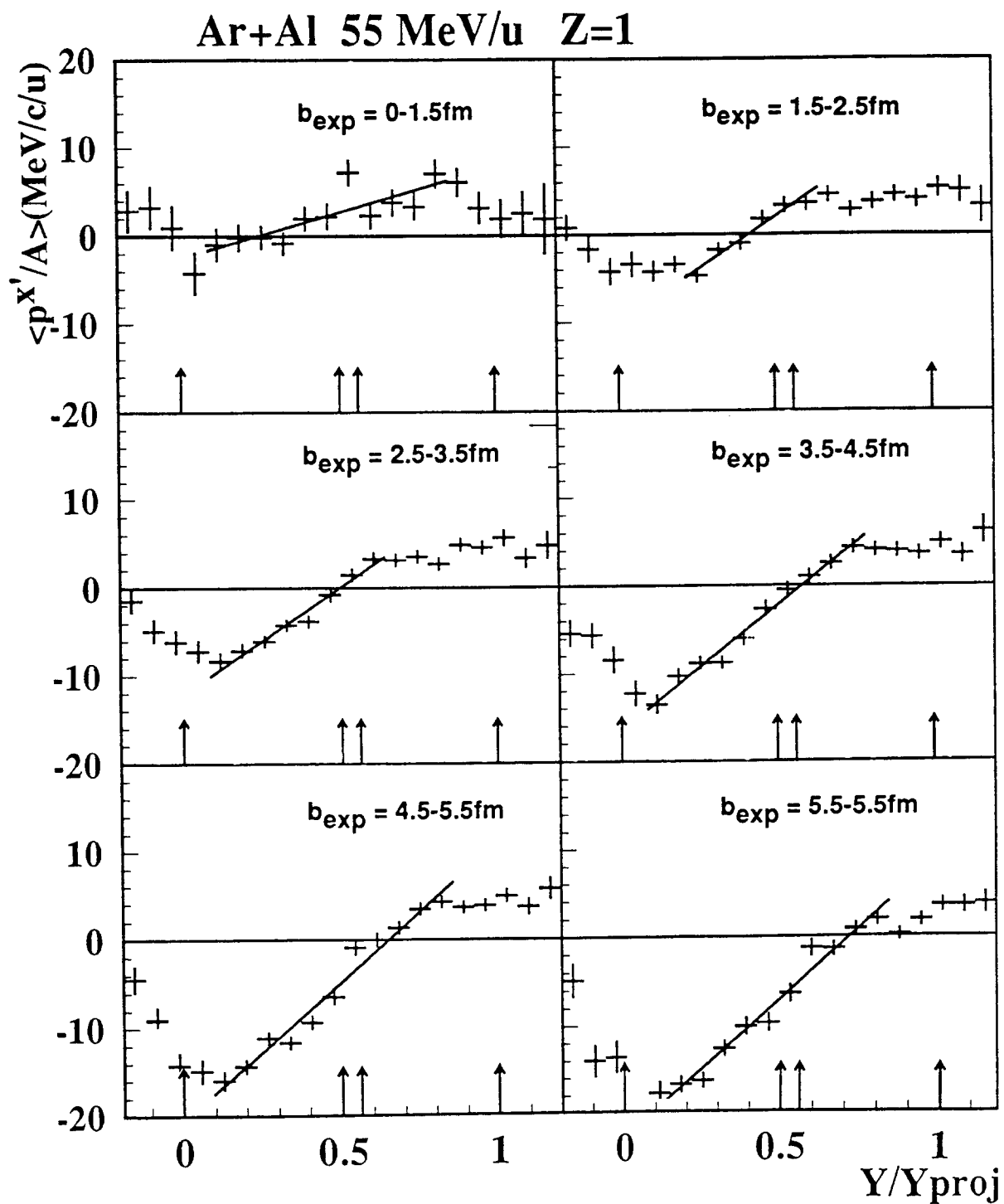
Figure 7: Average in plane transverse momentum per nucleon distributions versus rapidity for Z=1 particles and the incident energy E=55 MeV/u. Each pannel corresponds to an interval of experimentally determined impact parameter.
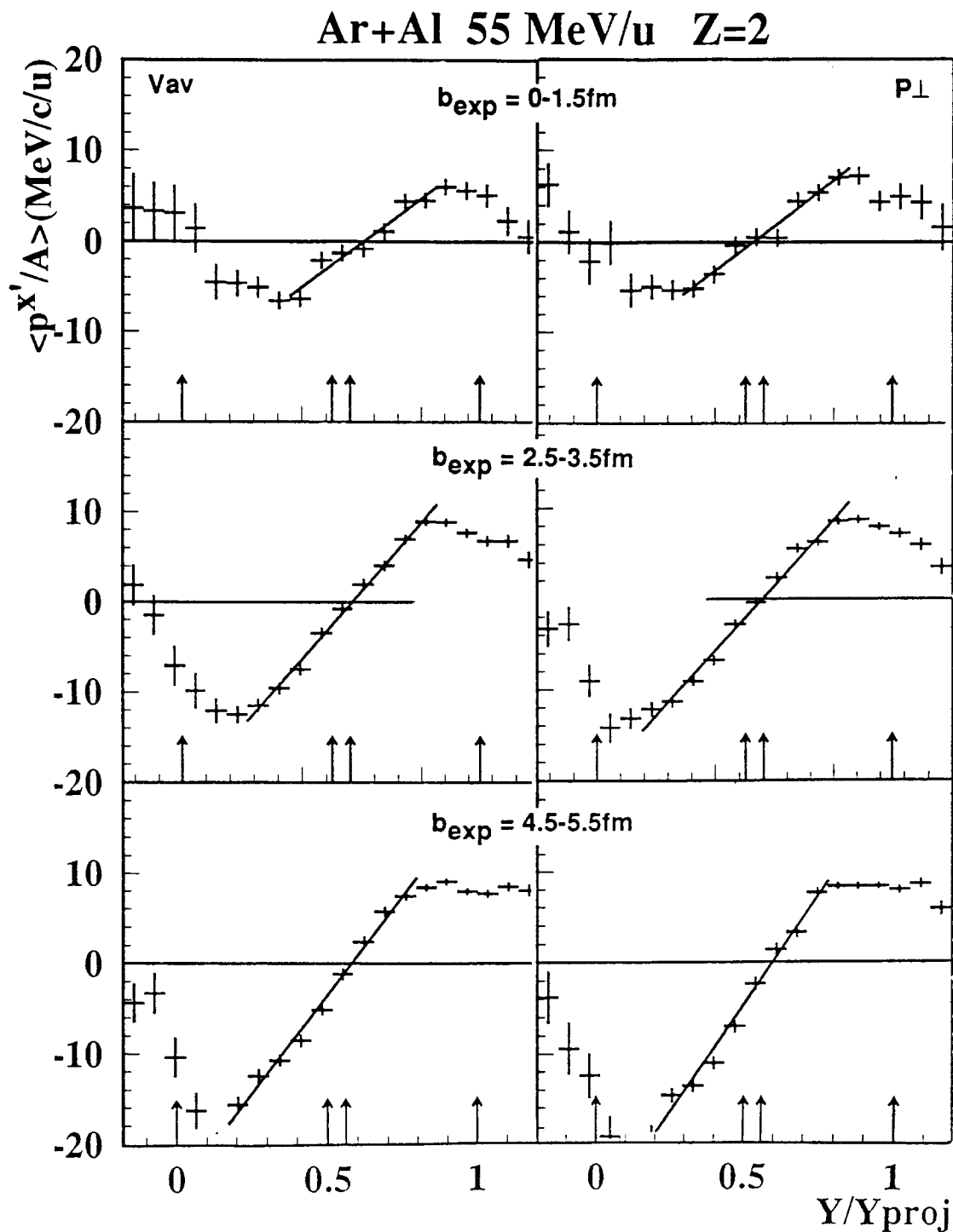
Figure 8: Average in plane transverse momentum per nucleon distributions versus rapidity for Z=2 particles at 55 MeV/u for three interval of b_{exp} . In the left column, the impact parameter sorting was done with V_{av}. It was done with $P_{\perp}$ in the right column.
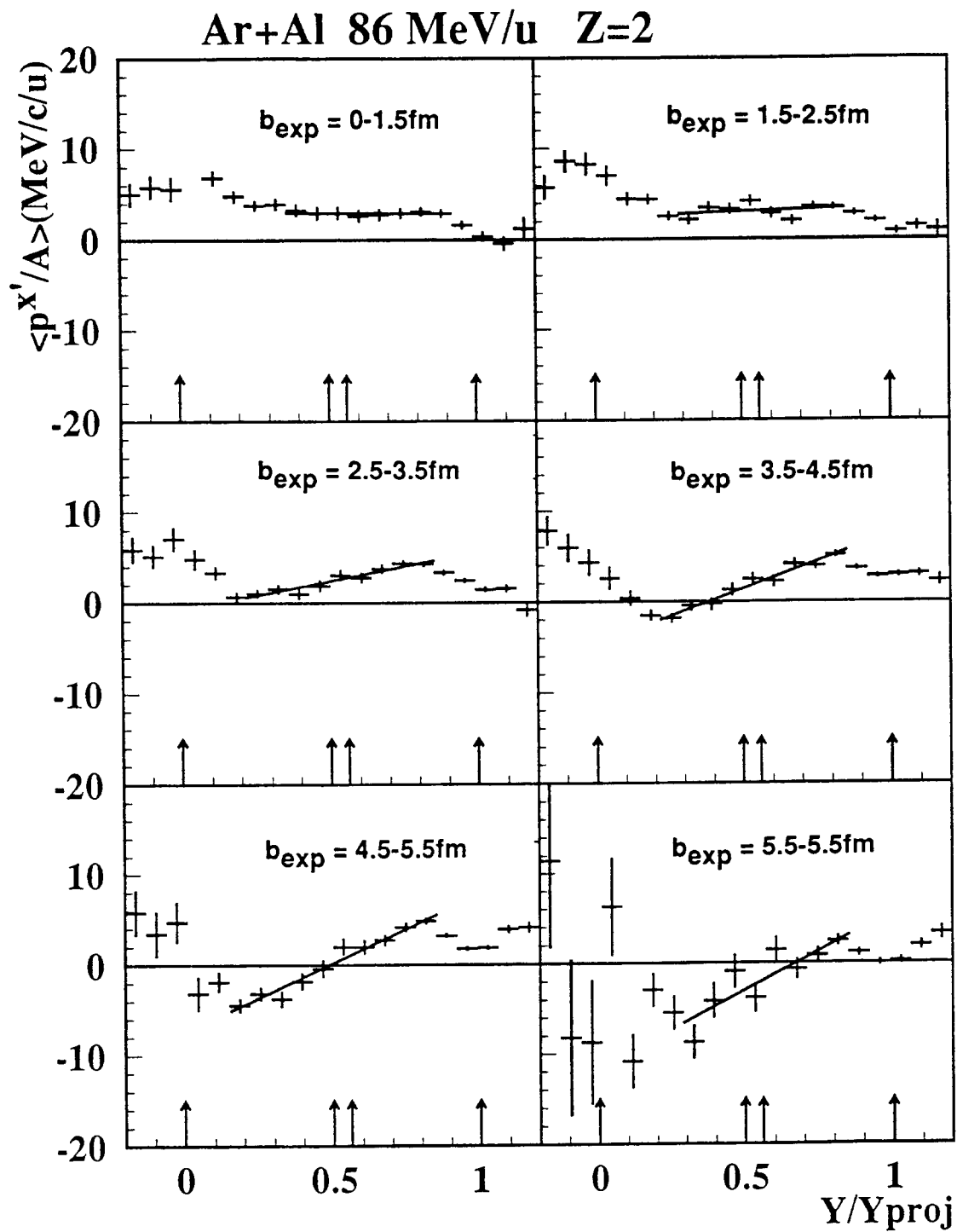
Figure 9: The same as fig. 7, but for E=86 MeV/u incident energy and for Z=2 particles.
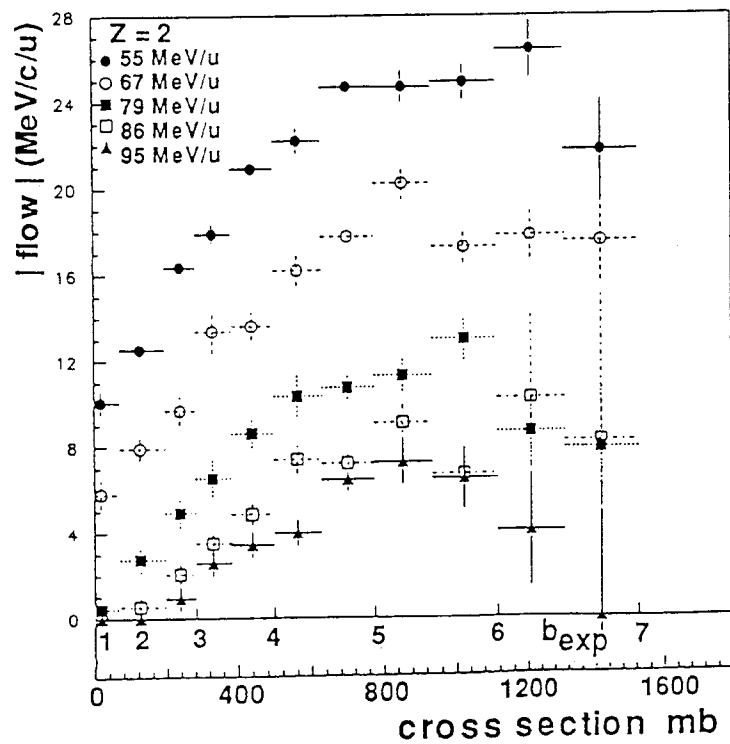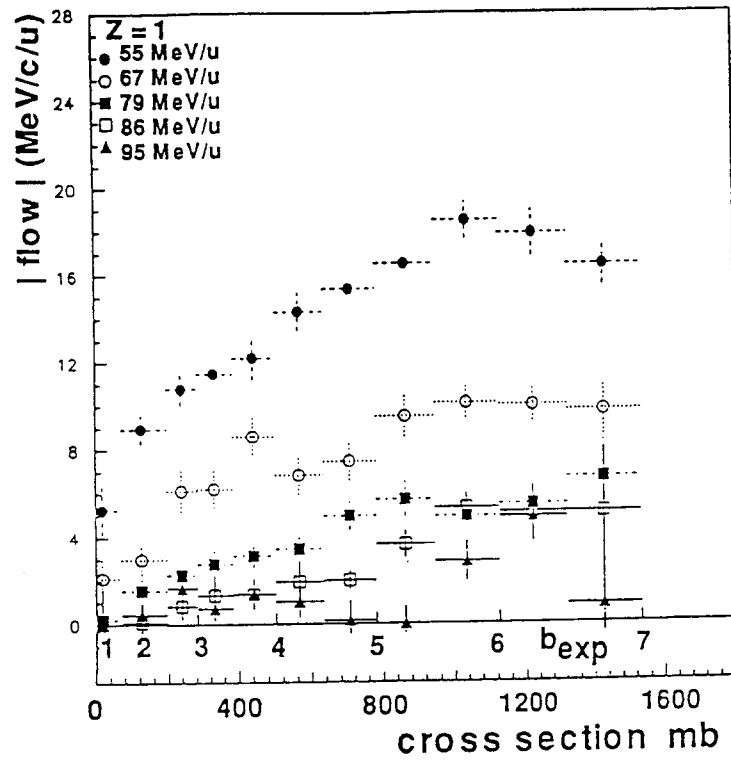
Figure 10: Impact parameter dependence of the flow parameter for Z=1 (upper pannel) and Z=2 (lower pannel) and for the five energies studied in this report. The impact parameter sorting was done with the average parallel velocity, V_{av}.
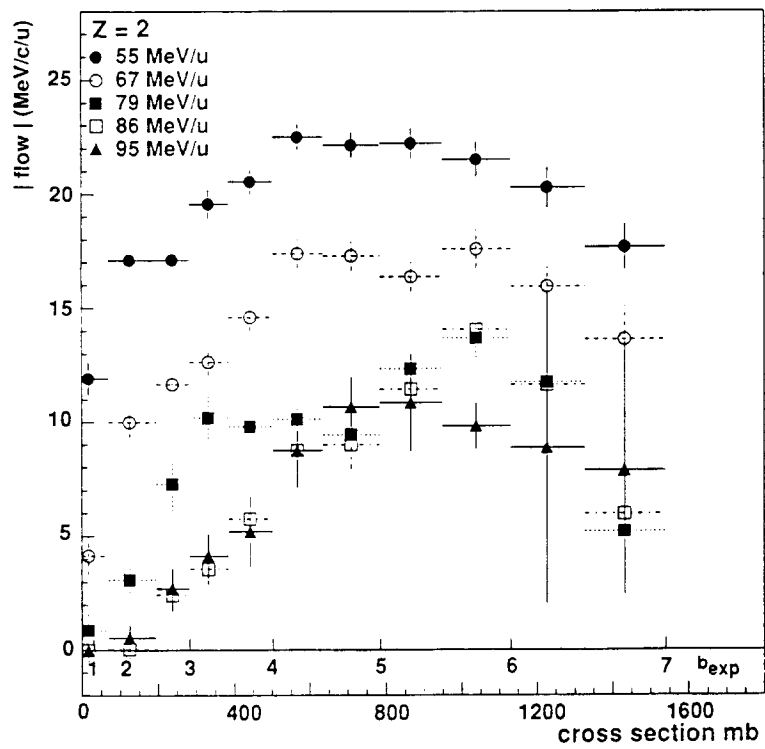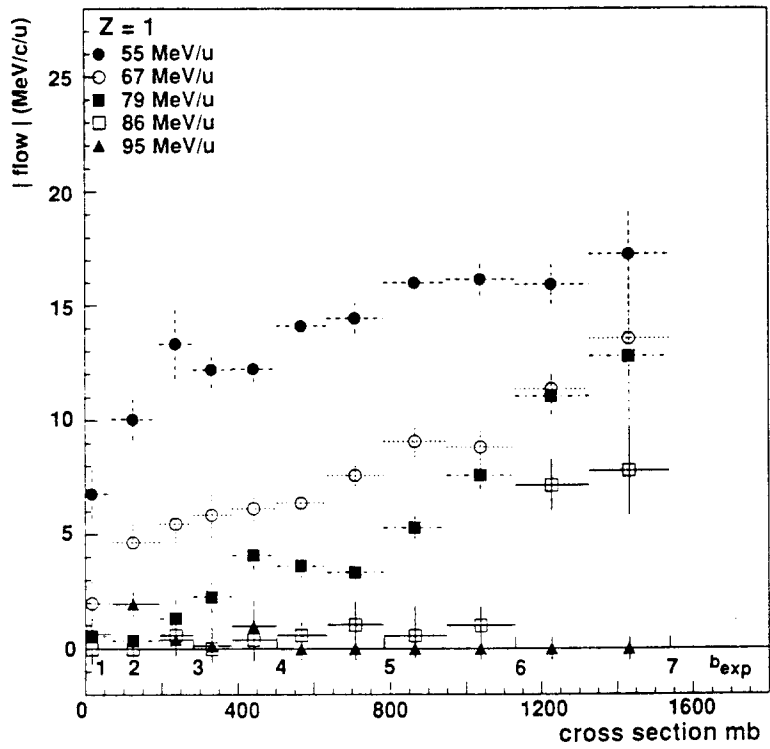
Figure 11: The same as fig. 10, but the impact parameter sorting was done using the total transverse momentum, $P_\perp$.
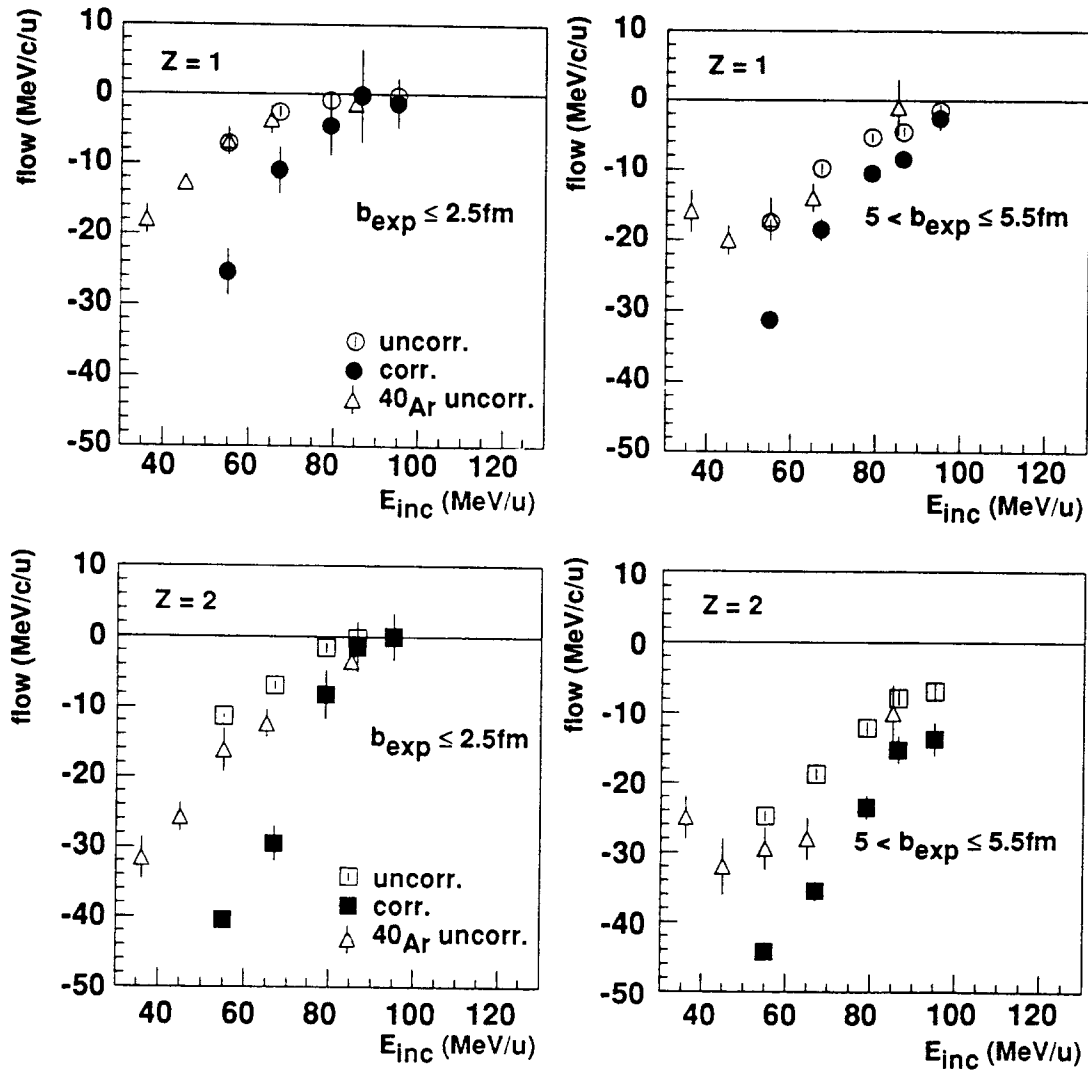
Figure 12: Energy dependence of the flow parameter for particles with Z=1 (upper pannels) and Z=2 (lower pannels) for two intervals of impact parameters mentionned in each pannel. There are shown both, uncorrected flow values and values corrected for the uncertainties related to the reaction plane reconstruction.
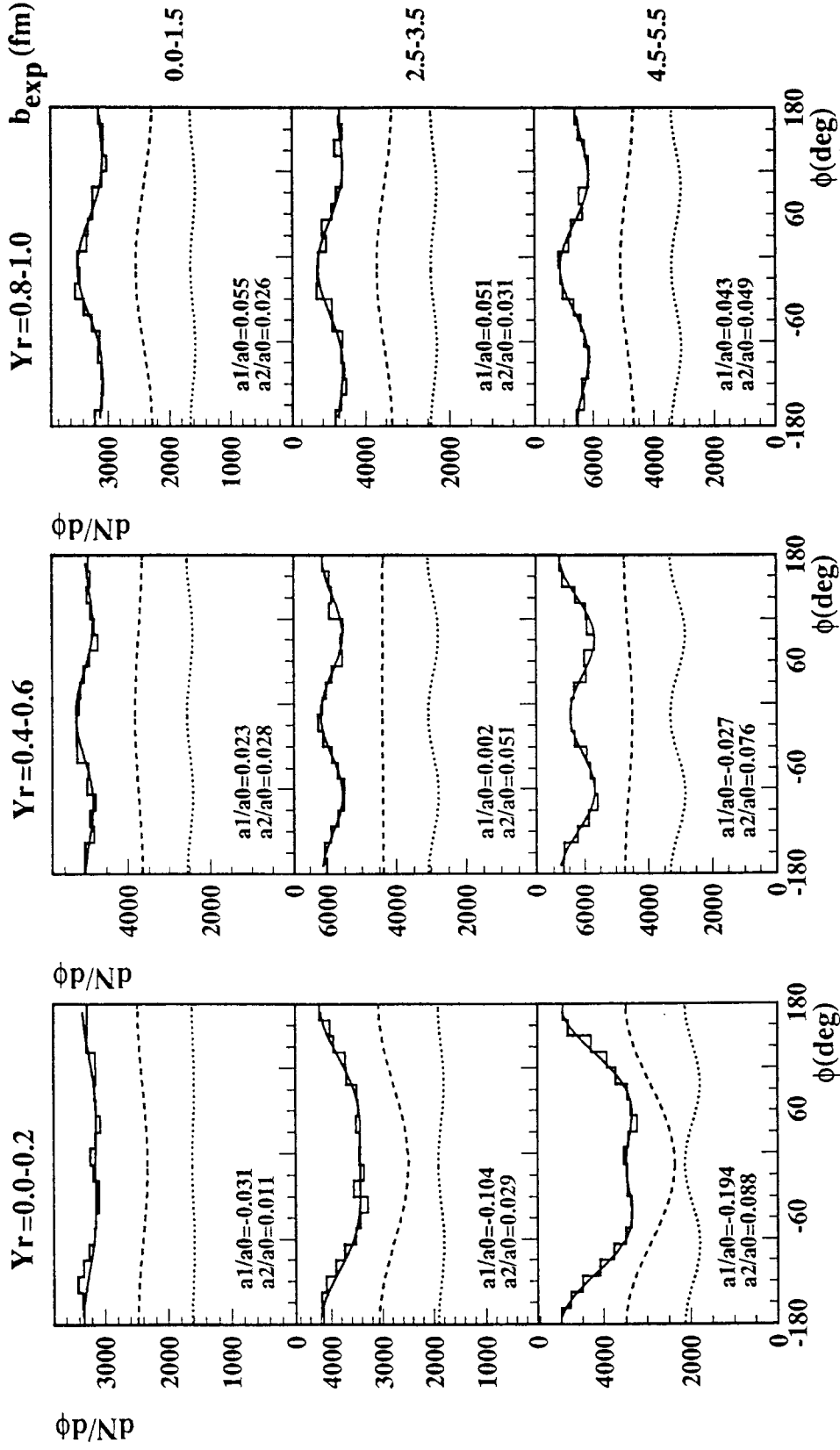
Figure 13: The *azimuthal* distributions of particles with Z=1 for the incident energy E=55 MeV/u, three intervals of rapidity and three intervals of impact parameters mentionned on the figure. The solid curves are fits with formula (6) to the data and the ratios $a1/a0$, $a2/a0$ are values resulting from the fit. The meaning of the other two curves in each pannel is explained in the text.
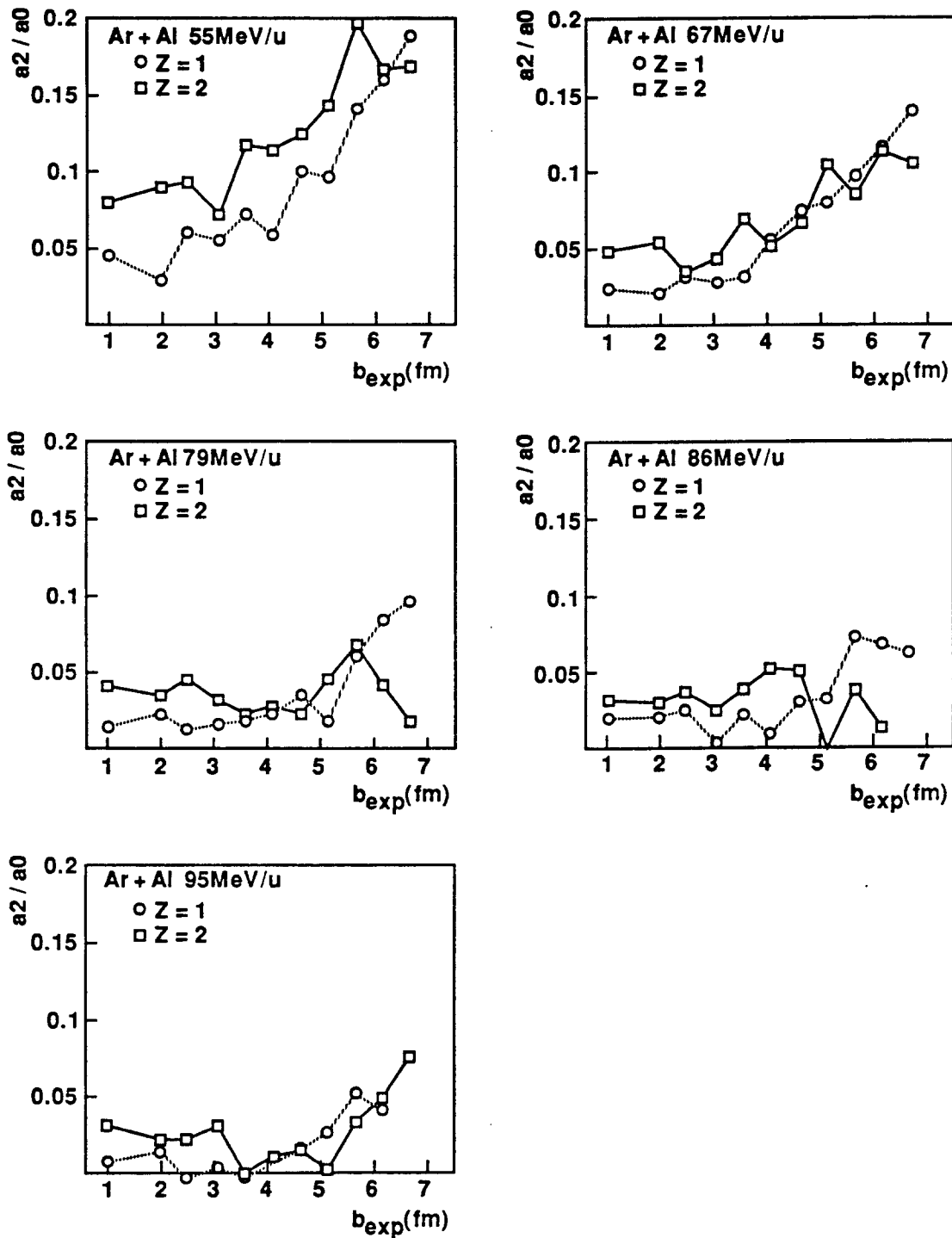
Figure 14: Impact parameter dependence of the ratio $a2/a0$ (see text), for the five experimental energies mentioned in each pannel . At each incident enegy are shown distributions for both, Z=1 and Z=2 particles.